Upgrading the Lyon Cluster Ion Accelerator by a Radiofrequency Quadrupole

H. O. Moser, A. Schempp

Institut für Kernverfahrenstechnik

Kernforschungszentrum Karlsruhe

KERNFORSCHUNGSZENTRUM KARLSRUHE

Institut für Kernverfahrenstechnik

KfK 4201

Upgrading the Lyon Cluster Ion Accelerator by a Radiofrequency Quadrupole

by

H. O. Moser and A. Schempp[*]

KERNFORSCHUNGSZENTRUM KARLSRUHE GMBH, KARLSRUHE

[*]   Institut für Angewandte Physik der Universität Frankfurt/Main, Robert-Mayer-Str. 2-4, D-6000 Frankfurt/Main

Nachrüstung des Lyoner Clusterionen-Beschleunigers mit einem Radio-
frequenz-Quadrupol

Zusammenfassung

Der Entwurf eines RFQ mit variabler Endenergie, der geeignet ist, Cluster-
ionen vom elektrostatischen Clusterionen-Beschleuniger in Lyon nachzube-
schleunigen in den Massenbereichen 1 bis 25 u bzw. 1 bis 50 u auf kine-
tische Energien von 1.32-2.5 MeV bzw. 2.64-5.0 MeV im Dauerstrich- bzw.
Pulsbetrieb, wird vorgestellt. Zusätzlich wird ein Strahlführungssystem,
das den elektrostatisch vorbeschleunigten Strahl mit Hilfe von zwei elek-
trostatischen Quadrupoltriplets an den RFQ anpaßt, beschrieben. Auch ohne
RFQ dient dieses Strahlführungssystem der Verbesserung der Strahlparameter
auf dem Target, wie z. B. der Teilchenstromdichte oder der Strahldivergenz.
Eine Abschätzung der Kosten des Projektes führt zu etwa DM 345 000.- bzw.
FF 1 200 000.- zuzüglich Mehrwertsteuer.

Upgrading the Lyon Cluster-Ion Accelerator by a Radiofrequency Quadrupole

Abstract

The design is presented of an RFQ with variable final energy suitable to
post-accelerate cluster ions from the Lyon electrostatic cluster-ion
accelerator in the mass ranges from 1 to 25 u and 1 to 50 u up to kinetic
energies of 1.32-2.5 MeV and 2.64-5.0 MeV for cw and pulsed operation,
respectively. Furthermore, a beam line is described which matches the
electrostatically preaccelerated beam to the RFQ by use of electrostatic
quadrupole triplets. When used without RFQ this beam line serves to improve
beam parameters on the target, such as the particle flux density or beam
divergence. The estimated costs of this project are about DM 345 000.- or
FF 1 200 000.- without VAT.

Introduction

The Lyon cluster-ion accelerator was initated 15 years ago within the frame
of a collaboration between the Institut de Physique Nucléaire de Lyon and
KfK as part of a project conducted by KfK and aimed at the development of
intense hydrogen cluster-ion beams for nuclear fusion /1/. After completion
of the fusion-oriented work in 1978, and in particular during the past few
years, this accelerator has seen a growing experimental activity (for
references see /2/). In order to widen the available range of beam para-
meters, and to improve the performance, a possible upgrading is studied
which includes, as the most important part, an RFQ as a post-accelerator
and a new beam line to transport the beam from the exit of the acceleration
gap to the target or the entrance of the post-accelerator.

RFQ parameters

A first example of a 4-rod-λ/2-RFQ accelerating cluster ions for basic
research is discussed in /2/. Compared to this design the basic parameters
were modified in order to comply with budget constraints. The final energy
was halved to 2.5 MeV in cw operation which shortens the RFQ to about 3 m
length. Using a standard 20 kW FM transmitter a kinetic energy of 100 keV/u
is possible within the mass range of 1 to 25 u in cw operation, or within 1
to 50 u in the pulsed mode. The latter case corresponds to a final energy
of 5 MeV. Since the input cluster-ion beam is already pulsed, the pulsed
operation of the RFQ does not mean a serious restriction. An overview of
the major parameters is given in Table 1. Figure 1 displays

Table 1: RFQ parameters

Initial kinetic energy per u	keV	10
Final kinetic energy per u	keV	100
Maximum total kinetic energy	MeV	2.5(5)
Maximum ion mass	u	25 (50)
Length of structure	m	2.96
Clear aperture between electrodes	mm	4
Number of cells		281

Initial length of cell ($\beta\lambda/2$)	mm	6.4
Maximum modulation of electrodes		1.8
Diameter of vacuum chamber	m	0.5
Frequency	MHz	108
Peak voltage	kV	50(100)
Power	kW	20 (80)
Maximum field strength	MV/m	2.3(4.6)
Duty cycle		1.0(0.25)

Radial phase advance per cell		13 °
Initial longitudinal phase after shaper		-30 °
Final longitudinal phase		-20 °
Final longitudinal phase spread		±22 °
Final relative energy spread	%	± 1.1
Transmission	%	58
Normalized acceptance	mrad·mm	3

(Values in parentheses are valid for pulsed operation)

the longitudinal dependence of some parameters of interest.

A spectacular confirmation of the validity of the 4-rod-RFQ principle was obtained very recently by the Frankfurt group. A 1.2 m long 202.5 MHz 4-rod RFQ was installed at the HERA injection beam line at DESY and accelerated up to 35 mA of H$^-$ ions from 18 keV to 750 keV. The final energy spread was ±15 keV to be compared with ±13 keV at 20 mA as computed with PARMTEQ. The measured emittance was 1·π·mm·mrad in pretty good agreement with the PARMTEQ result of 1·π·mm·mrad (90 % beam). After conditioning of the resonator tank the design value of 20 mA was reached within one hour. Despite the low duty factor of this machine (pulse length 0.25 ms, repetition rate 1 Hz) the results show that the specific design of the electrodes and the resonator was successful and that the accelerator performance was quite insensitive to the operating conditions.

A new feature which is a prerequisite of the use as an accelerator for basic research purposes has been included. This is the possibility to vary the final energy. Up to now, RFQs have been fixed energy accelerators with, at most, very small variations of the final energy such as with the

proposed decelerator at CERN /3/. For the RFQ outlined in this report we take advantage of the dependence of both the resonance frequency and the shunt impedance, on the geometric parameters of the four-rod structure, as shown in figs. 2 and 3 /4/. The resonance frequency can be appreciably tuned so that it seems possible to scan the FM range from about 80 MHz to 110 MHz, corresponding to an energy change by a factor of 1.89. The maximum final energy of 2.5(5.0) MeV would be obtained with 110 MHz, the minimum being 1.32(2.64) MeV at 80 MHz. The shunt impedance and power would vary between 250 and 380 kOhm/m and 30(120) and 21(84) kW, respectively. The height H of the main current loop (Fig. 3) was chosen as variable parameter. An experimental embodiment of its variation is currently investigated in order to prove the practical usefulness of this approach.

Further perspectives

With the RFQ designed for 1 - 50 u and 100 keV/u final energy with a 80 - 110 MHz transmitter heavier cluster ions can be accelerated by choosing smaller values of frequency and final energy per mass unit. The scaling laws connecting the mass number N with the frequency f and final energy E_{uf} are $N \cdot f^2$ = const and $N \cdot E_{uf}$ = const, respectively. A rather cheap way to obtain the mass range of 1 to 10^3 u with an initial energy and a final energy of 0.5 keV/u and 5 keV/u, respectively, would be to modify the transmitter and the structure such that they work between 17.9 and 24.6 MHz. The option for this modification may be included when the transmitter will be ordered. This mass range comprises cluster ions with, e.g. 1000 hydrogen atoms, 62 oxygen atoms, 17 nickel atoms or 9 silver atoms. For an analysis of the mass range 1 to 10^6 u see ref. /2/.

Since the total energy of 5 MeV is about the limit for RFQs, at least at present, further increases would call for other accelerating schemes. In this context, low-velocity superconducting linear accelerating structures which appear to be useful and available from β = 1 % to higher values /5/ might be of help. Even further acceleration by circular accelerators is conceivable /6/.

Beam transport from acceleration gap to target or RFQ entrance

A schematic of the existing beam line is displayed in fig. 4. The beam is accelerated vertically, then bent into the horizontal direction by a cylindrical electrostatic deflector (74°) and a bending magnet (16°). The purpose of the magnet is to provide mass selection. Apart from the weak focussing due to the deflector and the magnet in the radial plane and some edge focussing through the tilted pole faces of the magnet (see below), the beam line has not contained focussing elements so far. To improve the beam transport, the effect of quadrupole triplets added to the beam line was analysed (fig. 5). The objective of the first triplet is to optimize the beam transport across the deflector and the magnet, while the second triplet serves to match the phase space occupied by the beam to a desired condition on the target or to the acceptance of an RFQ post-accelerator.

Electrostatic quadrupoles are chosen for two reasons. Firstly, as the velocity of 10 keV-protons is 1.38×10^6 m/s corresponding to $\beta = 0.46$ %, an electric field strength of 13.8 kV/cm is equivalent to a magnetic flux density of 1 T ($E = vxB$). Thus, an electrostatic field is still rather effective. Secondly, the first triplet has to be placed in a quite restricted space inside the high vacuum, and electrostatic quadrupoles lend themselves more readily to comply with these restrictions.

Method of beam optics calculation

Since the emittance of the cluster ion beam at the exit of the acceleration gap is not known a rather large value was assumed for the calculation, namely $\pi \cdot 5$ mm·5 mrad. Then the non-linear optics and tracking code MARYLIE /7/ was used to trace 20 rays and to look at the phase space plots at 6 selected planes intersecting the design orbit perpendicularly. These planes are located at the entrance, the center, and the exit of the electrostatic deflector, at the exit of the bending magnet, and at 0.1 m and 1.05 m downstream of the second triplet. The phase space plots in these planes permit to follow the transport of the beam through the individual beam line elements.

Since MARYLIE's catalogue of beam line elements contains neither the electrostatic deflector nor the electrostatic quadrupole, a separate program, MPDOME, was written to calculate the maps describing these beam line elements. More details on this procedure will be given in a further report.

The following results were obtained using only the linear part (transfer matrix) of the map.

Additional focussing components

Figure 6 displays the geometry of the quadrupole triplet used. The electrostatic potential ψ is given by

$$\psi = (U_0/r_0^2)(y^2-x^2)$$

where 2 U_0 is the voltage between rods of opposite polarity and r_0 is the distance between the axis and the pole tips. If $U_0 < 0$, the quadrupole is focussing in x-direction and defocussing in y-direction, and vice versa for $U_0 > 0$. The x-coordinate lies in the plane containing the beam line, while the y-coordinate is perpendicular to that plane. The central quadrupole is focussing in the x-direction, leading and trailing quadrupoles in the y-direction. It has already been taken into account that the cross-section of the electrodes is not hyperbolic, but cylindrical in order to make fabrication easier. According to /8/, the radius of the cylinders is 1.16 r_0 giving a radial distance of the electrode axes from the quadrupole axis of 2.16 r_0. Figure 7 shows the focal lengths in x- and y-directions, respectively, for the 1-2-1 triplet versus the parameter U_0/r_0^2. The focal length is extracted from the transfer matrix (see, e.g., /9/). If the components of the phase space vector are (x,p_x,y,p_y,t,p_t), then the matrix elements m_{21} and m_{43} are related to the focal lengths f_x and f_y by the relations

$$f_x = -1/m_{21} \quad \text{and} \quad f_y = -1/m_{43}.$$

The triplet is fed by two high-voltage supplies featuring positive and negative output polarities.

As a consequence of the geometry chosen the focal lengths are different in the same sense over the whole interval. This is a desired feature since the beam waist should be in the center of the deflector, for the x-direction, and in the magnet, for the y-direction (cf fig. 5). Thus, the triplet must be oriented in such a way that the short focal length applies to the x-direction, and the long one to the y-direction.

Phase space evolution during beam transport

The following figs. 8 - 10 show phase space plots in the 6 planes of section. The upper plot of a column displays x and p_x as abscissa and ordinate, respectively, while the center and the lower plots represent (y,p_y) and (t,p_t) in a similar way. From the two ellipses shown in a plot that at the orthogonal position gives the initial conditions in the cathode. The evolution of the emittance can thus always be compared with the initial situation. The plots are normalized to the maximum values of the coordinates as given in the table on top. Three typical cases of beam transport are analysed, namely, the "neutral" beam transport, where the shape of the phase space ellipses at the target close to the initial one, the case "parallel on target", where a small divergence angle on the target is favoured at the expense of a larger cross-section, and the case "focus on target", where a small spot on the target is favoured at the expense of a larger divergence angle. The settings of the triplets are given in table 2.

Table 2: Triplet settings

	neutral	U_0/r_0^2 parallel	focus	
triplet 1	2.5×10^7	2.5×10^7	2.5×10^7	V/m^2
triplet 2	6.9×10^6	5.38×10^6	1.24×10^7	V/m^2
(electro-		5.24×10^6	1.38×10^7	
static)				
triplet 2	10.0	7.8	18.0	T/m
(magnetic)	-10.0	-7.6	-20.0	

(The first row of triplet 2 holds for the central quad, the second row for leading and trailing quads.)

For $r_0 = 0.01$ m we obtain $U_0 \leq 2.5$ kV. In the last rows of table 2 the values of the gradient of the magnetic flux density are given for the case that the second triplet is a magnetic one. Apart from purely computational reasons for inserting a magnetic triplet there, the actual location would not preclude using a magnetic triplet. The relationship between the gradients of the electric and the magnetic fields is obtained by equating the forces on a particle. Using the expressions

$$\psi = (U_0/r_0{}^2)(y^2 - x^2)$$

for the electrostatic, and

$$A_z = (I_0/2)(y^2 - x^2)$$

for the vector potential, and setting

$$-\partial\psi/\partial x = v\partial A_z/\partial x,$$

we find

$$U_0/r_0{}^2 = -vI_0/2,$$

where v and I_0 are the particle velocity and the magnetic field gradient, respectively. Inserting $v = 1.38 \times 10^6$ m/s which holds for a 10 keV proton the electrostatic settings for triplet 2 in table 2 are computed. From fig.8 we see that the width of the x-p_x-ellipse in x-direction is always less than ± 5 mm in planes 1-3, indicating that the beam passes the deflector without exceeding its aperture. Correspondingly, the width of the y-p_y-ellipse in planes 3 and 4 is less than ± 12.5 mm, which means that the beam passes the magnet chamber without obstruction, too. The setting of the first triplet which determines the passage through the deflector and magnet, is kept constant for all three cases.

In the case of the "neutral" solution, the resulting phase space ellipses are pretty close to the initial ones.

In the case of the "parallel on target" solution, the position and the incidence angle vary in the ranges ± 8 mm and ± 3.5 mrad, respectively, for the x-coordinate, and ± 9 mm and ± 2.9 mrad, respectively, for the y-coordinate.

In the "focus on target" case the corresponding ranges for x,p_x and y,p_y are (± 1.56 mm, ± 16.4 mrad) and (± 1.6 mm, ± 14.8 mrad), respectively. This beam spot fits reasonably well the RFQ entrance with its 4 mm clearance. The corresponding emittances are about 81 mm·mrad and 75 mm·mrad, respectively. They fit largely the acceptance of 650 mm·mrad calculated by dividing the normalized acceptance given in table 1 by $\beta = 0.0046$. It should be noted that in this case the last plane is shifted

towards the triplet, the distance between plane #5 and plane #6 then being 0.2 m instead of 0.95 m.

Figure 11 illustrates chromatic effects in the beam line. Comparison of fig. 11 with fig. 10 in the plane #6 shows that a relative energy deviation of 10^{-4} leaves the position of the spot on the target almost unchanged while the range of impact angle is shifted by about 16 mrad from ± 16.4 mrad to 0-33 mrad. However, at the exit of the deflector (plane #3), the beam exceeds the acceptable aperture of ± 5 mm by about 3 mm and is lost at about 50 %.

Thus, it depends on the emittance of the real beam whether or not this loss occurs. It could be mitigated by either increasing the aperture of the deflector providing a new outer electrode with a larger radius, or by dividing the deflector into two parts and putting quadrupoles in between to realize an achromatic system, or by a broad-band feedback system causing the deflection voltage to follow the acceleration voltage to better than 10^{-4}.

Figure 12 serves to assess the influence of the pole face angle of the bending magnet. The pole faces are tilted by an angle of 4° from the radial position towards a parallel configuration. However, the catalogue of beam line elements of MARYLIE contains either normal-entry bending magnets (tilt angle 0°) or parallel-faced bending magnets (tilt angle = half of bending angle). All phase space plots were computed with the normal entry bend, except for those of fig. 12 which use the parallel-faced bend. The real situation, thus, is somewhere between figs. 12 and 10. Obviously, in a linear approximation, the influence of the pole face angle is small.

Costs

Since the 4-rod structure is comparably easy to manufacture the major costs are caused by the transmitter. A preliminary offer from a German manu-facturer quotes DM 215 000.- without value added tax for a fixed frequency transmitter (108.5 MHz). The option of varying the frequency between 80 and 110 MHz is estimated to cause an additional amount of DM 30 000.- without VAT. The modification of the transmitter to operate below 30 MHz is expected to require another DM 40 000.- without VAT. Estimating about DM 100 000.- for the manufacture of the structure, the tank and the vacuum

equipment, the order of DM 345 000.- or FF 1 200 000.- without VAT seems to be realistic for the variable energy RFQ without low frequency option.

References

/1/ E. W. Becker, H. D. Falter, O. F. Hagena, W. Henkes, R. Klingelhöfer, K. Körting, F. Mikosch, H. O. Moser, W. Obert, J. Wüst, Kernfor-schungszentrum Karlsruhe, Report KfK 2016, 1974; H.O. Moser, J. Martin, R. Salin, J. de Physique 38, C2-215(1977); E. W. Becker, H. D. Falter, O. F. Hagena, P. R. W. Henkes, R. Klin-gelhöfer, H. O. Moser, W. Obert, I. Poth, Fusion Technology, Pergamon Press, Oxford, 1979, p. 331; H. O. Moser, Kernforschungszentrum Karlsruhe, Report KfK 4068, 1986.

/2/ H.O. Moser, A. Schempp, Kernforschungszentrum Karlsruhe, Report KfK 4090, 1986; H.O. Moser, A. Schempp, to be published in Nuclear Instrum. Methods, April 1987.

/3/ J.H. Billen, K.R. Crandall, T.P. Wangler, M. Weiss, Proc. 3rd LEAR Workshop, CERN, Geneva, 1985, p. 107.

/4/ A. Schempp, H. Klein, H. Deitinghoff, P. Junior, M. Ferch, A. Ger-hard, K. Langbein, N. Zoubek, Proc. of the 1984 Linear Accelerator Conference, Seeheim, FRG, 1984, GSI 84-11, p. 100.

/5/ K.W. Shepard, Rev. Sci. Instrum. 57,770-772(1986).

/6/ G. Stein, unpublished.

/7/ A.J. Dragt, R.D. Ryne, L.M. Healy, F. Neri, D.R. Douglas, E. Forest, MARYLIE 3.0, A Program for Charged Particle Beam Transport Based on Lie Algebraic Methods, Program Manual, University of Maryland 1985; A.J. Dragt, E. Forest, J. Math. Phys. 24, 2734-2744 (1983).

/8/ I.E. Dayton, F.C. Shoemaker, R.F. Mozley, Rev. Sci. Instrum. 25, 485 (1954).

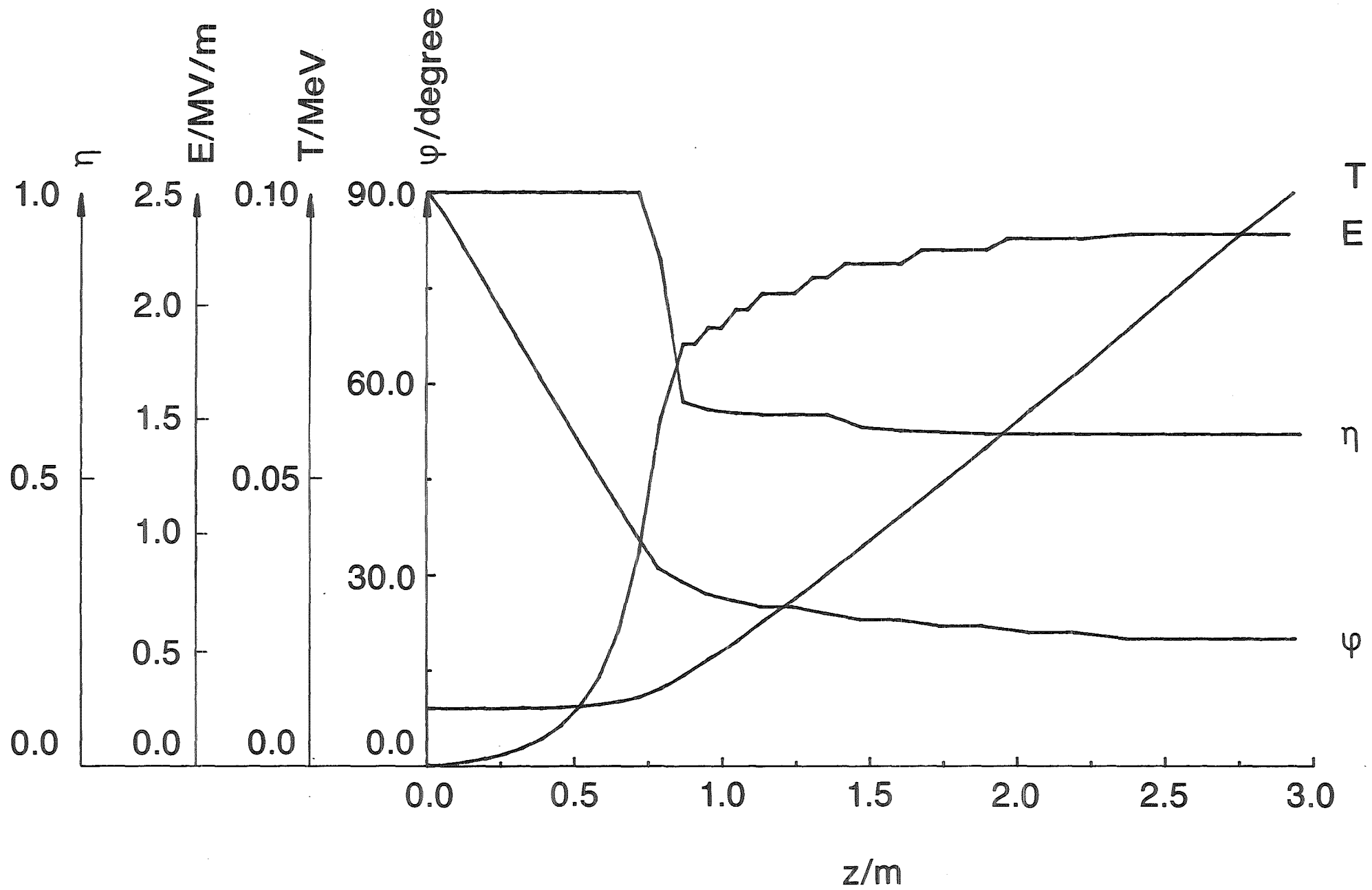/9/ E. Regenstreif, in A. Septier (editor), Focusing of Charged Par-ticles, Vol. I, Academic Press, 1967.

Fig. 1: Kinetic energy per mass unit u T, accelerating field strength Ez, phase φ, and transmission η versus position z along the RFQ.
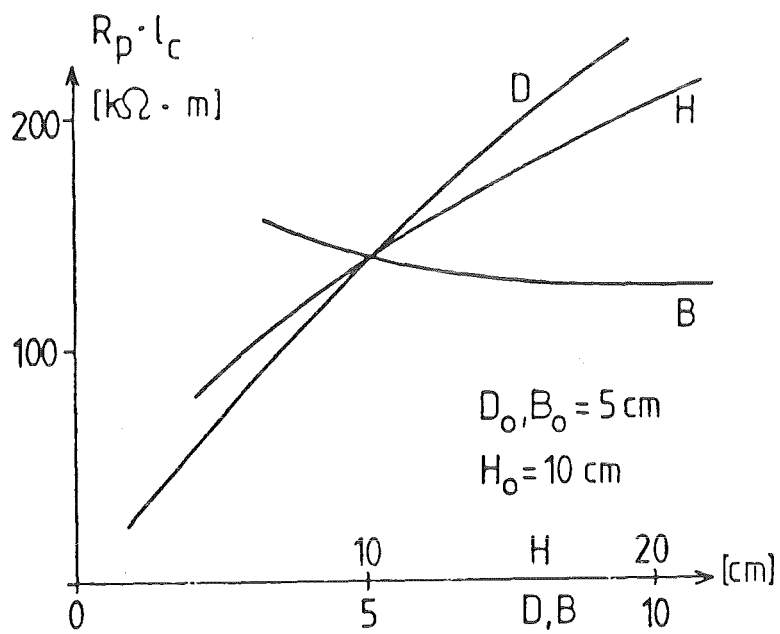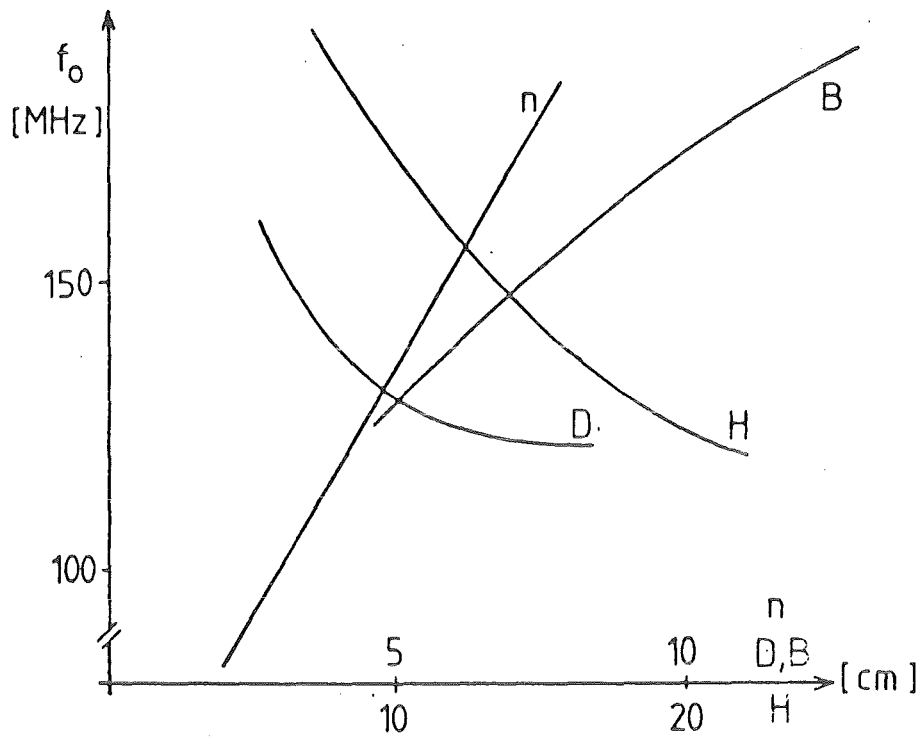
Fig. 2: Resonance frequency f_0 and shunt impedance R_S versus the height of the current loop H as illustrated in fig. 3.
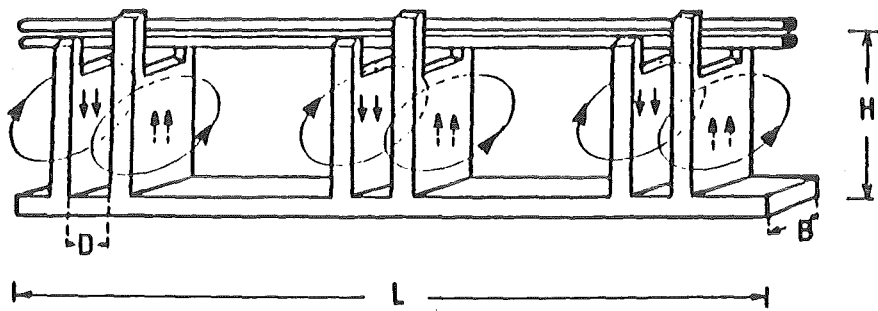
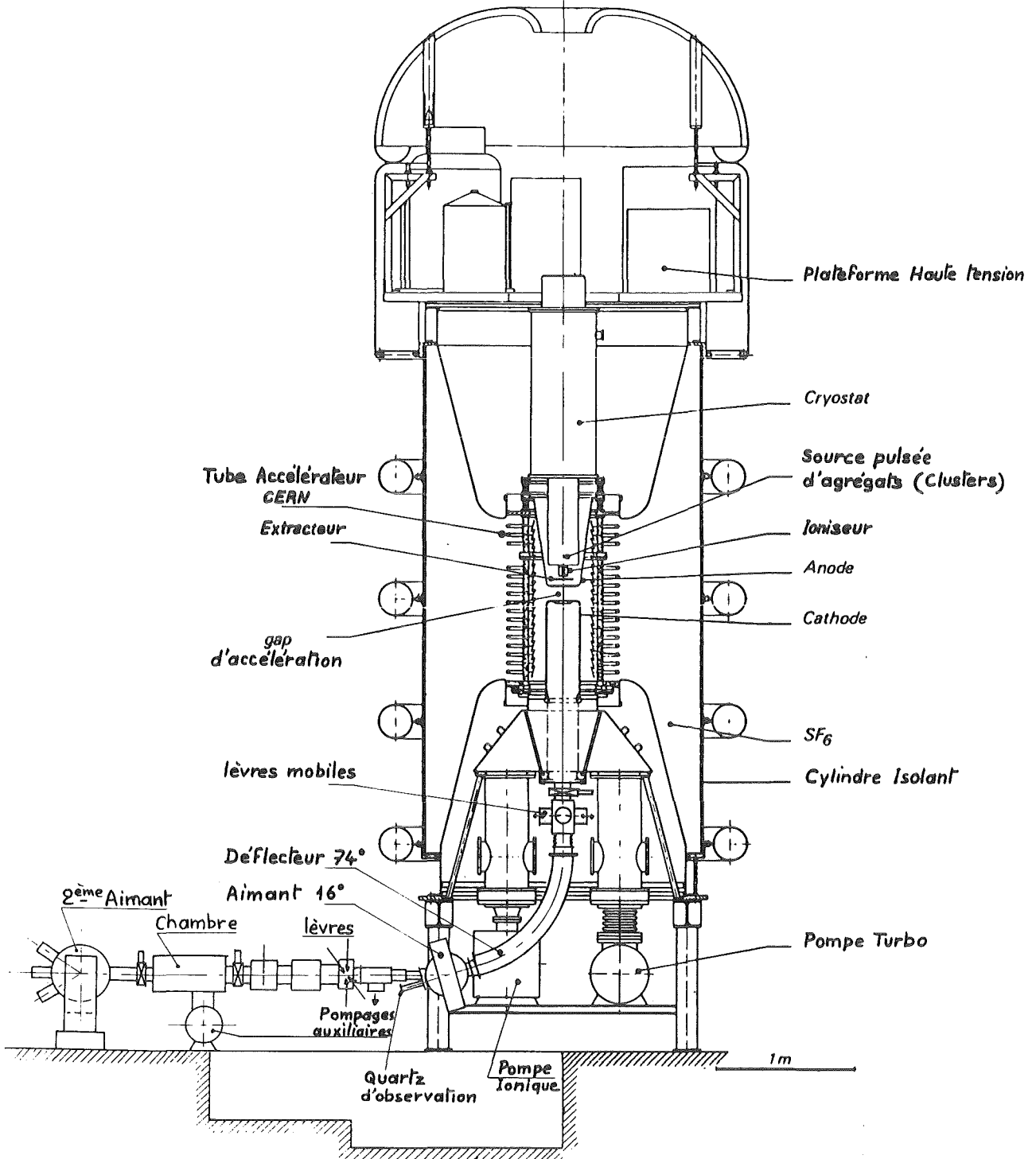Fig. 3:   Geometry of current loop in the 4-rod-λ/2-RFQ structure.

Plateforme Haute Tension

Cryostat

Source pulsée
d'agrégats (Clusters)

Tube Accélérateur
CERN

Ioniseur

Extracteur

Anode

Cathode

gap
d'accélération

SF₆

lèvres mobiles

Cylindre Isolant

Déflecteur 74°

2ème Aimant

Aimant 16°

Chambre

lèvres

Pompe Turbo

Pompages
auxiliaires

Quartz
d'observation

Pompe
Ionique

1 m

Fig. 4:   Schematic of existing beam line.

Beam line

0 [cm] Cathode

92.5

Triplet 1

122.5

167.5

74°

16°

Deflector

Bending magnet

r80

r100

Target or RFQ entrance
(30 in case of
"focus on target")

30

17.5

105

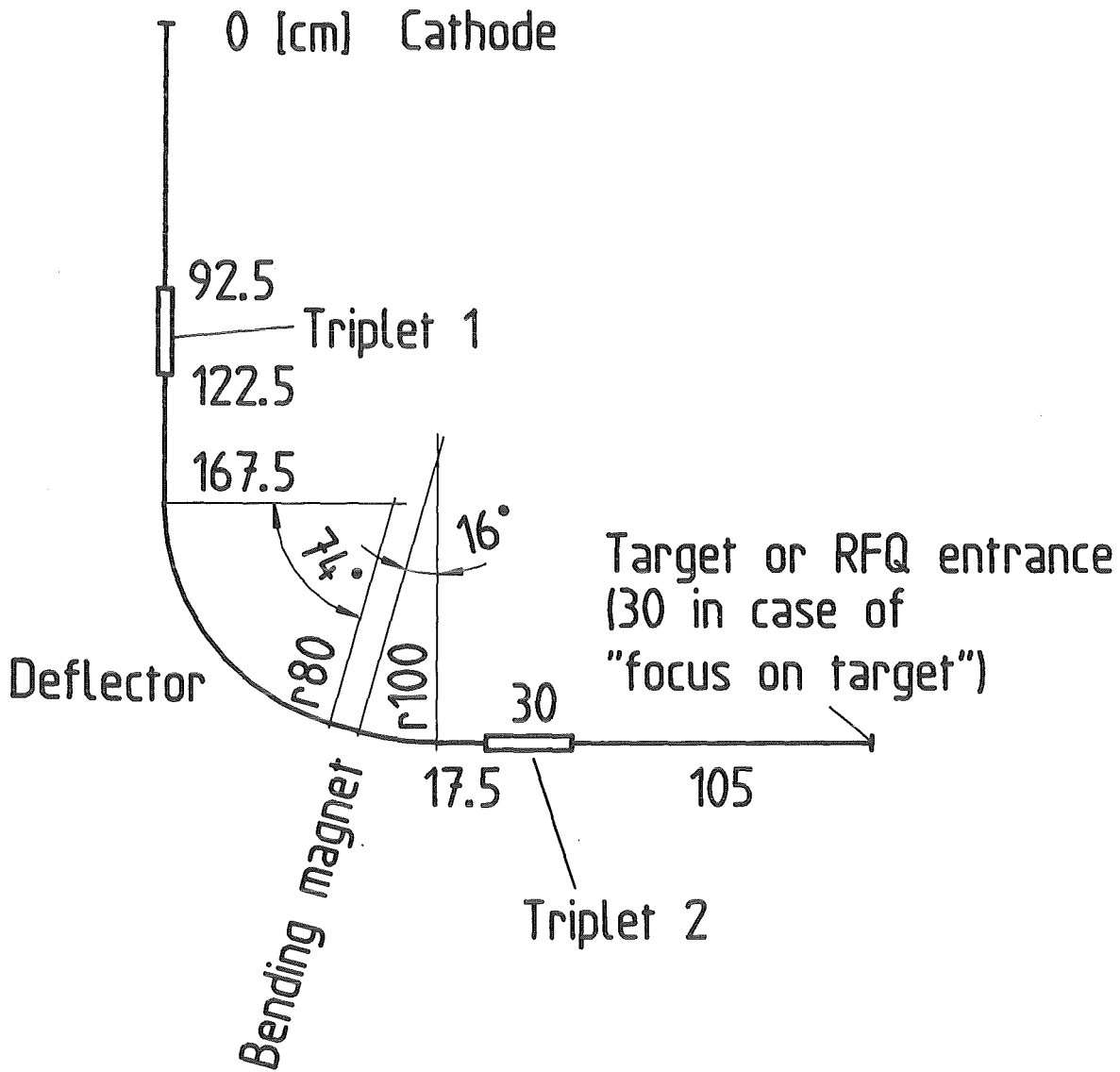Triplet 2

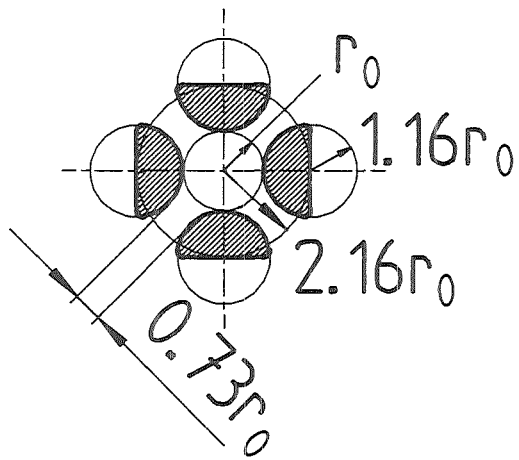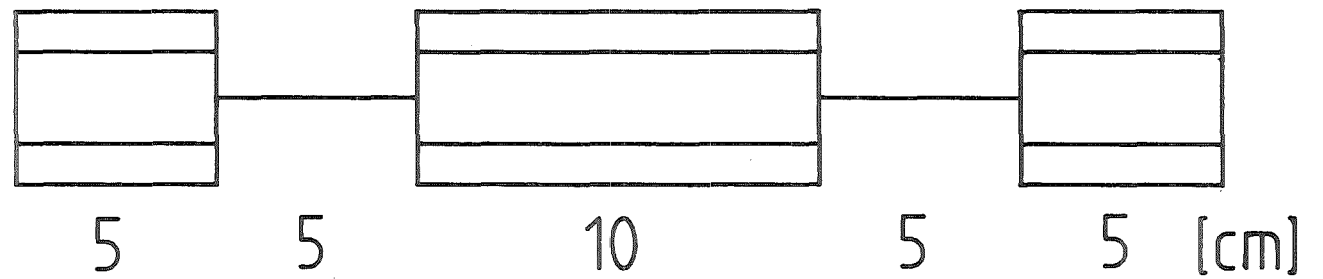CAD KfK F-V2-176-1286 IKVT

Fig. 5: Proposed new beam line with quadrupole triplets.

Quadrupole triplet

$r_0 = 1cm$

CAD   F-V2-175-1286 IKVT
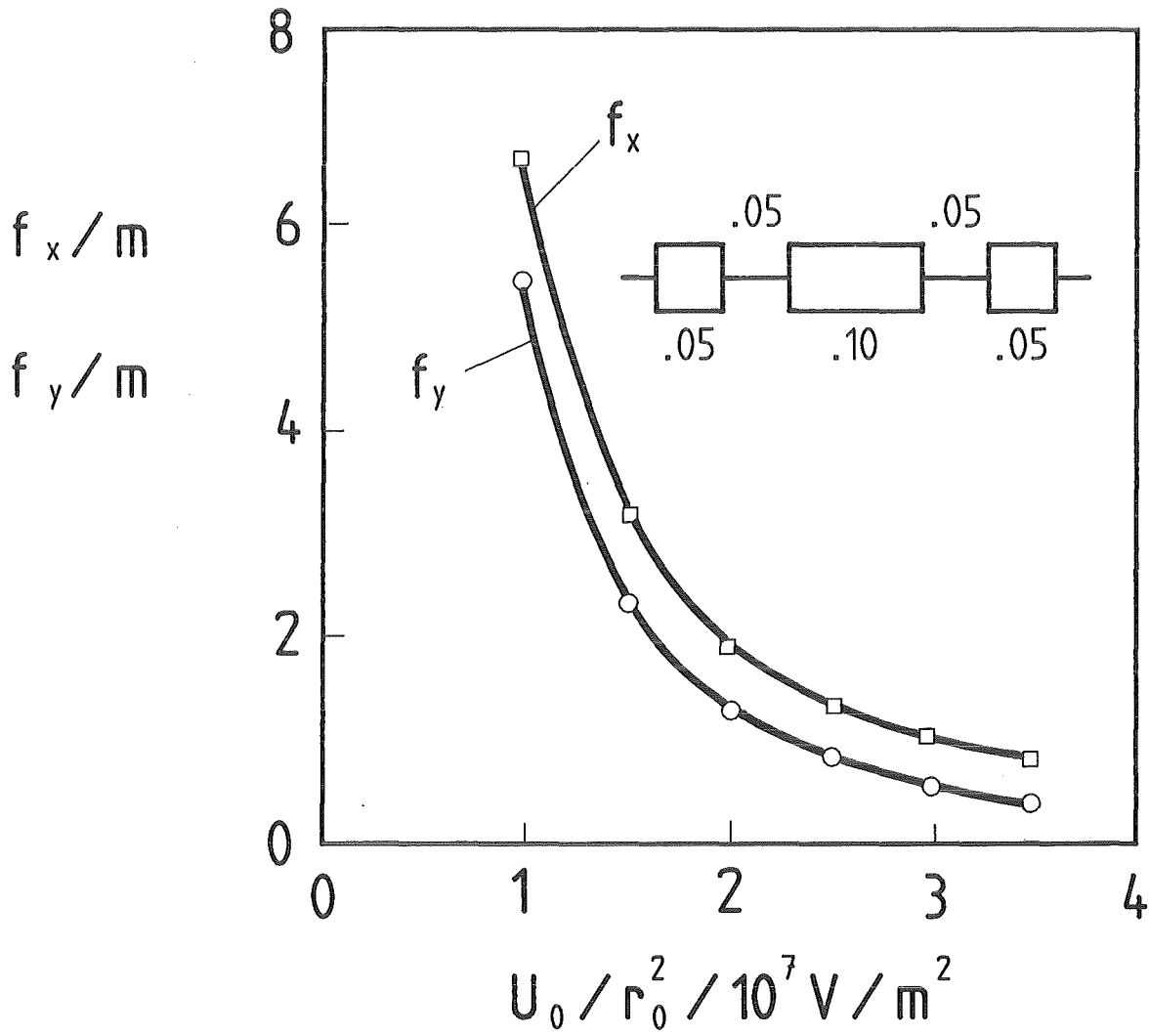
Fig. 6:   Geometry of quadrupole triplet.

Fig. 7: Focal lengths f_x, f_y versus quadrupole parameter U_0/r_0^2.

PLANE 1   PLANE 2   PLANE 3   PLANE 4   PLANE 5   PLANE 6

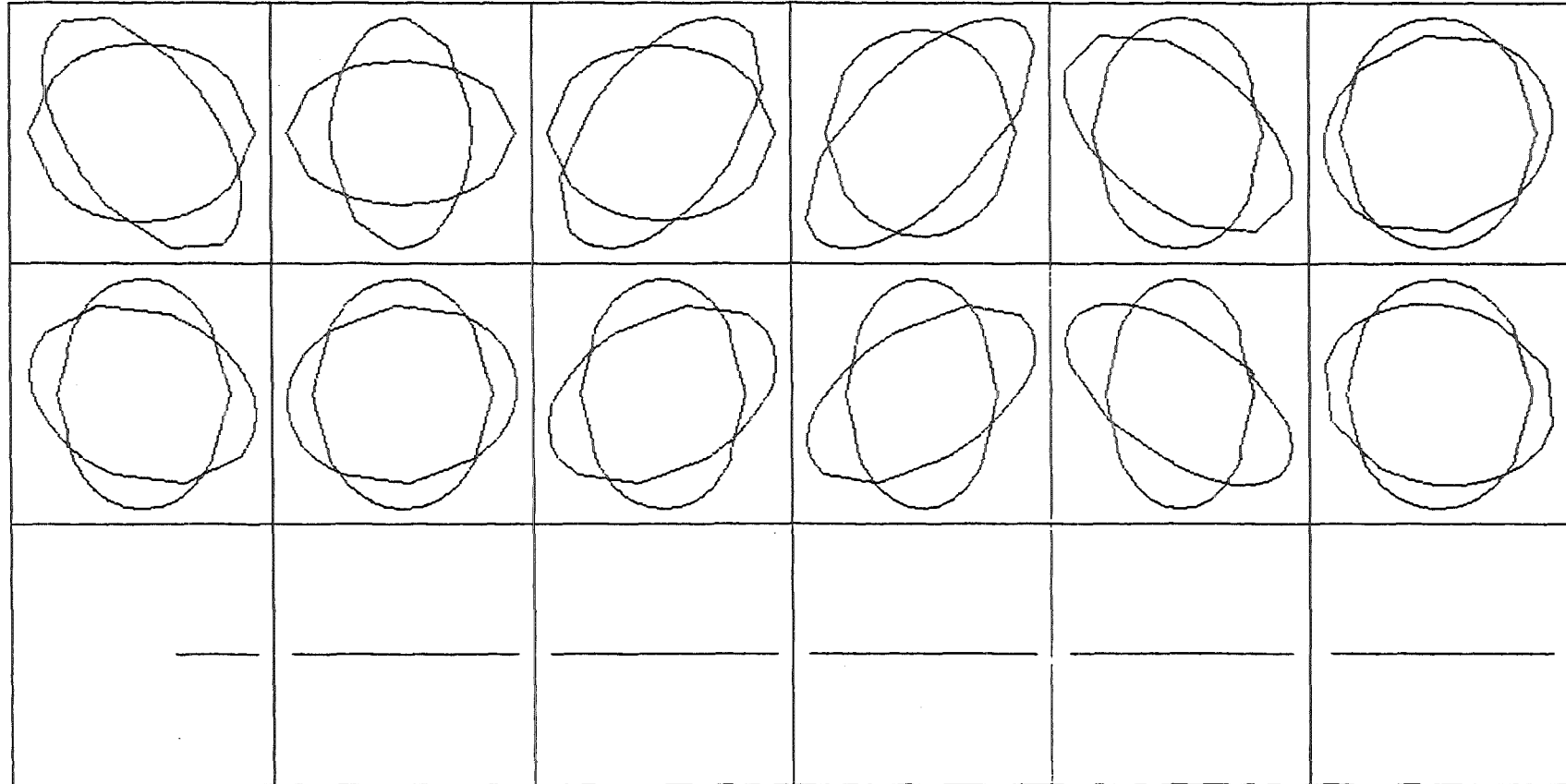|	PLANE 1	PLANE 2	PLANE 3	PLANE 4	PLANE 5	PLANE 6
XMAX	0.0050	0.0050	0.0050	0.0050	0.0057	0.0058
PXMAX	0.0055	0.0080	0.0066	0.0056	0.0050	0.0050
YMAX	0.0055	0.0054	0.0059	0.0076	0.0077	0.0061
PYMAX	0.0050	0.0050	0.0050	0.0050	0.0050	0.0050
TMAX	0.0038	0.1540	0.2531	0.2424	0.2442	0.2447
PTMAX	1.0000	1.0000	1.0000	1.0000	1.0000	1.0000

Fig.8: Phase space plots in six control planes for the case of approximately identical initial and final conditions.

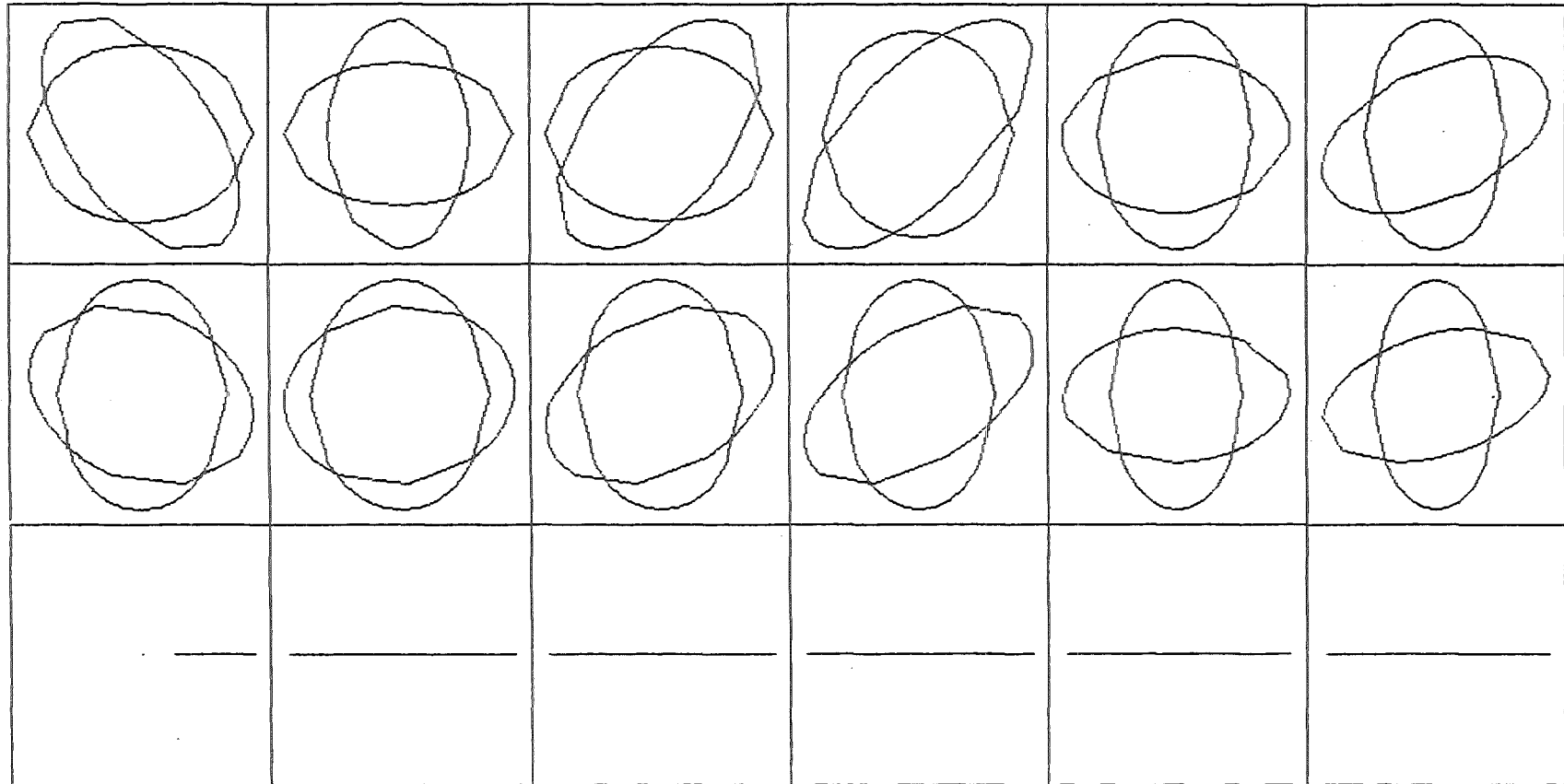| PLANE 1		PLANE 2		PLANE 3		PLANE 4		PLANE 5		PLANE 6	
XMAX	0.0050	XMAX	0.0050	XMAX	0.0050	XMAX	0.0050	XMAX	0.0072	XMAX	0.0080
PXMAX	0.0065	PXMAX	0.0080	PXMAX	0.0066	PXMAX	0.0056	PXMAX	0.0050	PXMAX	0.0050
YMAX	0.0065	YMAX	0.0064	YMAX	0.0069	YMAX	0.0076	YMAX	0.0084	YMAX	0.0090
PYMAX	0.0050	PYMAX	0.0050	PYMAX	0.0050	PYMAX	0.0050	PYMAX	0.0050	PYMAX	0.0050
TMAX	0.0038	TMAX	0.1540	TMAX	0.2531	TMAX	0.2424	TMAX	0.2437	TMAX	0.2440
PTMAX	1.0000	PTMAX	1.0000	PTMAX	1.0000	PTMAX	1.0000	PTMAX	1.0000	PTMAX	1.0000

Fig. 9: Phase space plots in six control planes for the case of a beam having low divergence on the target.

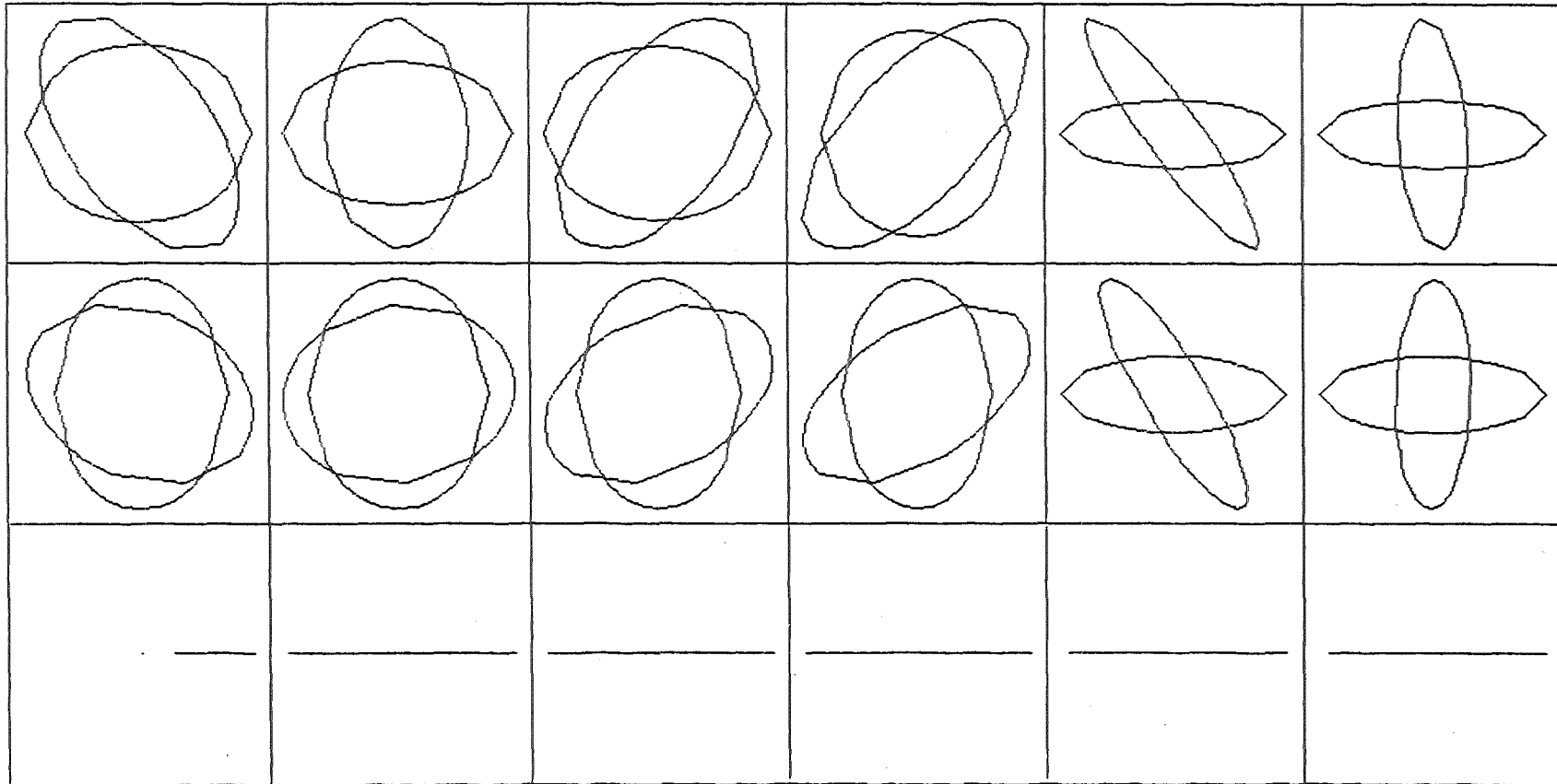| PLANE 1		PLANE 2		PLANE 3		PLANE 4		PLANE 5		PLANE 6	
XMAX	0.0050	XMAX	0.0050	XMAX	0.0050	XMAX	0.0050	XMAX	0.0050	XMAX	0.0050
PXMAX	0.0055	PXMAX	0.0080	PXMAX	0.0056	PXMAX	0.0056	PXMAX	0.0154	PXMAX	0.0164
YMAX	0.0055	YMAX	0.0054	YMAX	0.0059	YMAX	0.0075	YMAX	0.0050	YMAX	0.0050
PYMAX	0.0050	PYMAX	0.0050	PYMAX	0.0050	PYMAX	0.0050	PYMAX	0.0148	PYMAX	0.0148
TMAX	0.0038	TMAX	0.1540	TMAX	0.2531	TMAX	0.2424	TMAX	0.2485	TMAX	0.2501
PTMAX	1.0000	PTMAX	1.0000	PTMAX	1.0000	PTMAX	1.0000	PTMAX	1.0000	PTMAX	1.0000

Fig. 10: Phase space plots in six control planes for the case of a beam which is focused on the target.

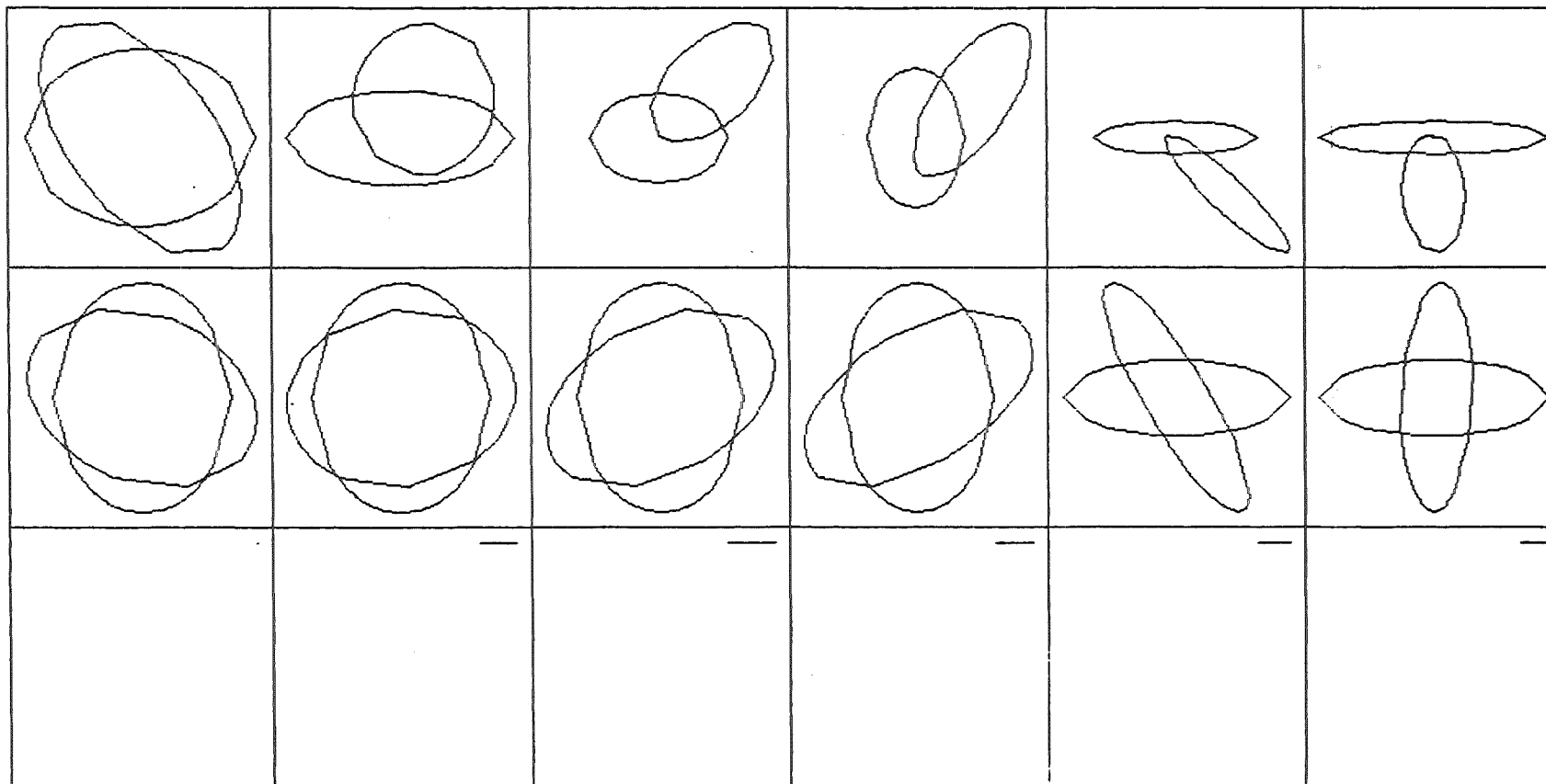| PLANE 1		PLANE 2		PLANE 3		PLANE 4		PLANE 5		PLANE 6	
XMAX	0.0050	XMAX	0.0050	XMAX	0.0083	XMAX	0.0117	XMAX	0.0059	XMAX	0.0050
PXMAX	0.0065	PXMAX	0.0121	PXMAX	0.0126	PXMAX	0.0083	PXMAX	0.0330	PXMAX	0.0330
YMAX	0.0065	YMAX	0.0054	YMAX	0.0069	YMAX	0.0075	YMAX	0.0050	YMAX	0.0050
PYMAX	0.0050	PYMAX	0.0050	PYMAX	0.0050	PYMAX	0.0050	PYMAX	0.0148	PYMAX	0.0148
TMAX	0.6093	TMAX	0.9842	TMAX	1.2208	TMAX	1.4892	TMAX	1.7855	TMAX	1.8848
PTMAX	0.0001	PTMAX	0.0001	PTMAX	0.0001	PTMAX	0.0001	PTMAX	0.0001	PTMAX	0.0001

Fig. 11: Chromatic effect. Influence of a 0.01 % relative energy deviation on the phase space patterns.

| PLANE 1		PLANE 2		PLANE 3		PLANE 4		PLANE 5		PLANE 6	
XMAX	0.0050	XMAX	0.0050	XMAX	0.0050	XMAX	0.0052	XMAX	0.0050	XMAX	0.0050
PXMAX	0.0055	PXMAX	0.0080	PXMAX	0.0055	PXMAX	0.0055	PXMAX	0.0155	PXMAX	0.0155
YMAX	0.0055	YMAX	0.0064	YMAX	0.0069	YMAX	0.0073	YMAX	0.0050	YMAX	0.0050
PYMAX	0.0050	PYMAX	0.0050	PYMAX	0.0050	PYMAX	0.0050	PYMAX	0.0145	PYMAX	0.0145
TMAX	0.0038	TMAX	0.1540	TMAX	0.2531	TMAX	0.2425	TMAX	0.2488	TMAX	0.2503
PTMAX	1.0000	PTMAX	1.0000	PTMAX	1.0000	PTMAX	1.0000	PTMAX	1.0000	PTMAX	1.0000
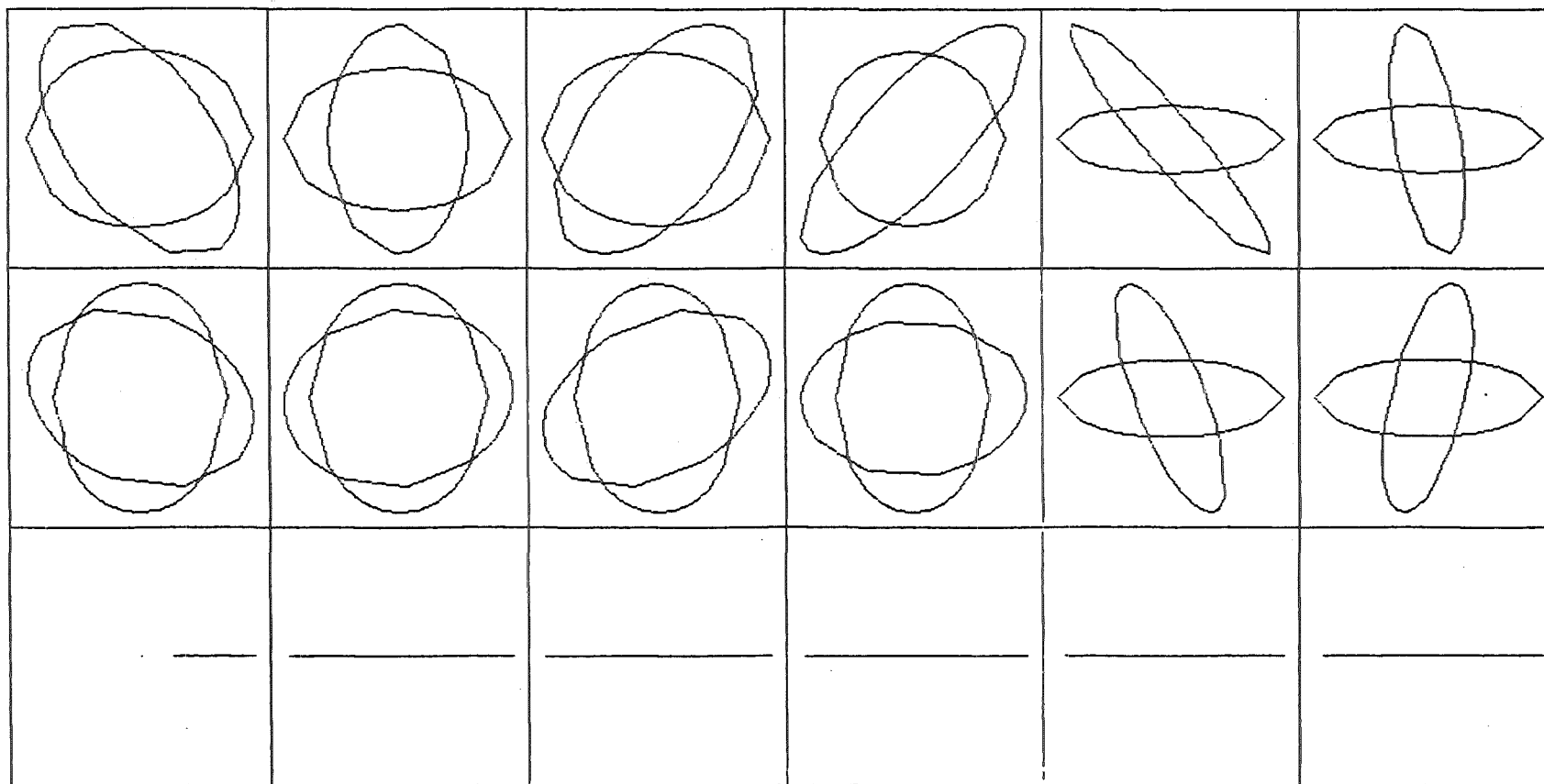
Fig. 12: Influence of the pole face angle of the bending magnet on the phase space patterns.